University of Groningen

Applied physics thesis

Modelling of Magnons

Journey Through Magnetic Moments and Frequencies

Author:
Hamza Reedy *(S4732073)*

Supervisors:
M.H. Guimaraes
Rixt Bosma

Abstract

Magnons present a promising path for information transfer in emerging areas such as magnonics and spintronics. Thus, modelling magnons through simulating magnetic samples with different parameters is a crucial step in understanding and utilizing them. This thesis delves into the dynamics of magnons and the precessional frequency of magnetic moments across a spectrum of sample shapes, dimensions, exchange stiffness, and magnetic field characteristics. Mumax3 was utilised to run simulations were FEM based on the LLG equation for modelling micro spins in a magnetic sample. Initial simulations uncovered unexpected trends attributed to experimental setups, particularly shape anisotropy and the direction of magnetic fields, which deviated from the Kittel formula's assumptions. Through systematic adjustments of parameters such as exchange stiffness and length, this work identifies critical factors influencing precessional frequency, highlighting the necessity of increasing exchange stiffness for homogeneity. The investigation extends to the simulation of thin films and cubic samples, exploring the impact of magnetic field strength and uniaxial anisotropy on magnonic behavior. Despite encountering methodological and computational limitations, the study achieves results within the theoretical range of the Kittel formula, with an error margin of 10%, from M_s and $M_{s,\text{fit}}$ difference. The study aimed to simulate a magnetic crystal with varying anisotropy constants and found consistent precessional frequencies across two domains, indicating a homogeneous macrospin influenced by high exchange length value. The study highlights potential in adjusting exchange stiffness and anisotropy in two-domain samples, providing insights into magnetic interactions and material design. Additionally, exploring out-of-plane effective fields in thin films could benefit spintronics research.

Contents

1 Introduction

The study of magnons and the precessional frequency of magnetic moments has a rich history, tracing back to the early 20th century when scientists first began to unravel the mysteries of magnetic phenomena at the microscopic level. Magnons, conceptualized as the quanta of spin waves, have since emerged as a cornerstone in the field of magnetism, offering deep insights into the behavior of magnetically ordered materials [1].

This area of research has evolved significantly over the years, with advancements in technology enabling more precise measurements and simulations of magnetic behavior in various materials [2]. Understanding how magnetic moments precess and interact under different conditions has been crucial in developing a wide array of magnetic devices, from traditional storage media like hard drives to cutting-edge applications in the realm of spintronics, where the spin of electrons, rather than their charge, is harnessed for information processing.

The exploration of how different shapes, dimensions, exchange stiffness, and magnetic field strengths and directions affect magnons and precessional frequencies is pivotal. Such studies enriches our fundamental understanding of magnetic dynamics. The aim of this research is contributing to this body of knowledge by systematically investigating these variables through simulations. Through this work, we hope to uncover new mechanisms and strategies for controlling magnetic phenomena, opening doors to novel technologies and materials that leverage the unique properties of magnons and magnetic moments. Adjusting the parameters within MuMax3 allows for accurate simulation of the predictions made by the Kittel formula. The aim is to model a magnetic crystal by having two alternating magnetic samples with an in-plane external magnetic field, as demonstrated in Figure 1), and then studying the precessional frequency of each sample macrospin.

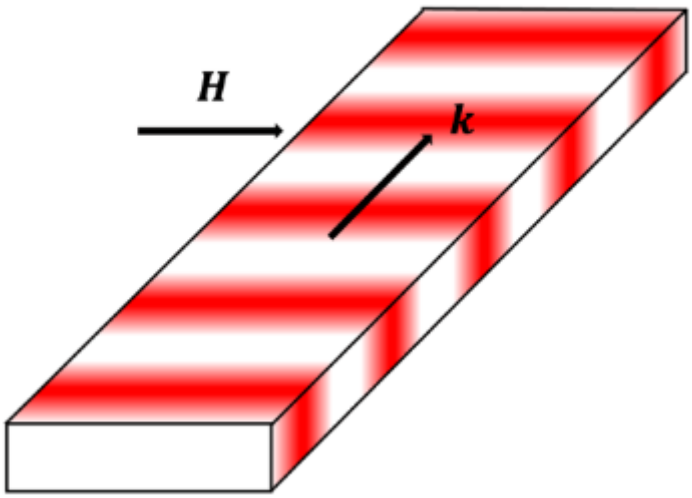

Figure 1: Visualization of two alternating samples with different anisotropies and an in-plane magnetic field. Different colors indicates different crystalline anisotropy constant. Adapted from [3]

2 Theory

2.1 Magnons and spin waves

A quasi particle is a concept in physics representing disturbances or excitation in a medium that behave as if they were particles. These entities can carry energy and momentum, exhibiting particle-like properties such as mass and charge, even though they are not actual particles in the traditional sense [4]. Magnons, a fascinating example of quasi particles, arise in the quantum description of magnetically ordered materials. Here, magnons will be explored, how they relate to spin waves and some of their practical applications [1].

Magnons , also referred to as spin waves, are collective excitation or quasi particles associated with the quantum-mechanical behavior of spins in a magnetic material [1], as visualised in Figure 2. In a magnetic solid, the orientation of electron spins tends to align, leading to magnetic order, primarily due to the quantum mechanical interaction known as the exchange interaction. This interaction is a consequence of the Pauli exclusion principle, which states that no two electrons can occupy the same quantum state simultaneously. When electrons are close to each other, their wave functions overlap, and the system lowers its energy by having the spins of these electrons align either parallel or antiparallel, depending on the type of exchange interaction (ferromagnetic or antiferromagnetic, respectively) [5]. Moreover, when the ordered state of spins within a material is disturbed by external factors like magnetic fields or thermal fluctuations, the spins may oscillate collectively. These oscillations, quantized into discrete units known as magnons [6], arise from a coherent precession of spins across the material. This requires a synchronized, collective movement, manifesting as wave-like behavior.

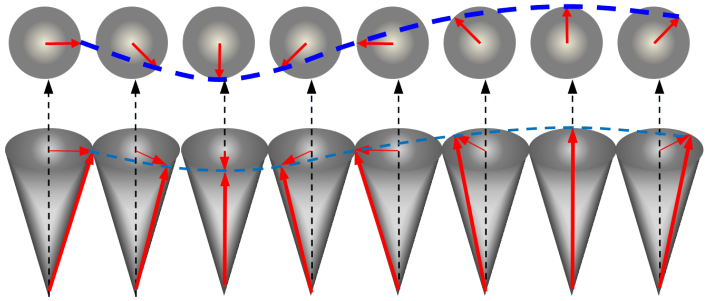

Figure 2: The image depicts two rows of spinning electrons with their spin directions represented by arrows. The top row shows individual electron spins misaligned with their neighboring spins, suggesting localized spin excitations. The bottom row illustrates a coherent wave-like pattern of electron spins, representing a magnon. Adapted from [7].

2.2 Information transportation

Magnons offer a promising avenue for information transportation in emerging fields like magnonics and spintronics. Magnonics is the study and manipulation of magnons to process and transmit information in wave-based computing systems [8]. Meanwhile, spintronics involves exploiting the spin of electrons, in addition to their charge, to develop electronic devices that offer enhanced performance for computing and data storage [9]. The unique quantum nature of magnons, coupled with their lack of charge and dissipation, presents advantages over traditional electronic methods. Magnons can propagate through magnetic materials with minimal energy loss, allowing for efficient information transfer. Manipulating magnons enables the encoding and transmission of information using spin waves, offering potential applications in magnonic devices. The ability of magnons to travel over extended distances with-

out significant loss makes them attractive for developing energy-efficient information transport mechanisms. For instance, multiferroic/ferromagnetic $BiFeO_3$ (BFO)/$La_{0.67}Sr_{0.33}MnO_3$ (LSMO) heterostructures have a decay length of up to one millimetre at room temperature [10]. They are capable of achieving extremely short wavelengths, reaching into the nanometer range, even at microwave frequencies [2]. Meanwhile, electromagnetic waves at microwave frequencies usually have wavelengths ranging from one meter down to one millimeter. This allows them to interact with a wide variety of other quantum excitations. Furthermore, their unique gyrotropic dynamics lay the groundwork for significant nonreciprocal behaviors, enabling directional control and manipulation in various applications.

Researchers are exploring innovative ways to harness magnons in spin-based technologies. Key to this field are magnonic devices which manipulate magnons through waveguides, guiding signals of specific frequency, wave vector, phase, and amplitude crucial for wave-based computing [11]. Innovative self-biased waveguides overcomes the limitations of needing a bias magnetic field for device integration, including exchange-coupled magnetic multi-layers and dipolar-coupled nanomagnet chains, offering enhanced functionality and enabling bias-free operations crucial for advancing nano-magnonics and magnonic-electronic hybrid technologies.

Moreover, magnons utilized in Yttrium Iron Garnet (YIG)-based devices, are applied in creating combinatorial logic and memory devices by exploiting their unique low magnetic damping [12]. These devices perform computations by identifying pathways between input and output ports, leveraging the parallel search capability of magnons for enhanced functionality. This approach demonstrates potential in enhancing computational throughput, potentially rivalling quantum computers in specific tasks [13], by utilizing the magnon's ability to navigate through multiple paths efficiently.

2.3 Controlling magnons through electrostatic gates

Electrostatic gates are a fundamental component in the control and manipulation of charge carriers in semiconductor devices, operating by applying an electric field that modulates the energy levels within the device, thus controlling the flow of electrons [14]. This principle is not confined to charge manipulation but extends to the realm of spintronics. In this context, magnons emerge as pivotal players. Magnons can be influenced by electric fields in materials where magnetic and electric properties are coupled, a phenomenon that becomes particularly intriguing when considering a magnetic sample.

The interaction between an electrostatic gate and a magnetic sample can be understood through the modulation of magnon energies and densities. This is because the electric field from the gate can affect the magnetic anisotropy and exchange interactions within the magnetic sample, thus altering the magnon spectrum [15]. For instance, the use of voltage gates to control magnon dispersion has been proposed as a mechanism for tunable magnonic devices [16], where the magnon bandwidth and propagation characteristics can be dynamically adjusted through electrostatic gating.

These advancements underscore the significance of electrostatic gates not just in traditional electronics but in the burgeoning field of spintronics and magnonics, suggesting a convergence of disciplines that could redefine information technologies. The ability to control magnonic currents through electrostatic gating of a magnetic sample represents a promising avenue for developing novel computational and memory devices that leverage the dual nature of electrons ,charge and spin, for enhanced performance and functionality.

The electric control of optically-induced magnetization dynamics in the van der Waals ferro-

magnet $Cr_2Ge_2Te_6$ (CGT) is modulated through electrostatic gating [17]. By employing top and bottom gates to independently adjust the charge carrier density and electric displacement field, significant alterations is shown in magnetization precession amplitude and internal effective fields. This manipulation reveals the substantial impact of coherent opto-magnetic phenomena beyond previously known thermally-induced mechanisms, indicating a promising method for tuning magnetic properties and dynamics. The dual-gate setup enables nuanced control over the CGT's magnetic parameters, paving the way for advancements in ultra-fast opto-magnonic devices and highlighting the potential of 2D ferromagnetic semiconductors in quantum computing and spintronic applications.

2.4 Landau-Lifshitz-Gilbert equation

The Landau-Lifshitz-Gilbert (LLG) equation is a fundamental equation in magnetism that describes the dynamics of magnetization in ferromagnetic materials. It plays a crucial role in understanding the precession, damping, and overall motion of magnetic moments or spins in response to external perturbations.It is extensively used in micromagnetic simulations and studies of magnetic materials, providing insights into phenomena such as spin precession, magnetization switching, and the response of magnetic systems to external stimuli. The equation is foundational in the design and analysis of spintronic devices, magnetic memory storage, and other technologies where the dynamic behavior of magnetization is crucial. The LLG equation is given by [18]:

$$\frac{d\mathbf{M}}{dt} = -\gamma \mathbf{M} \times \mathbf{H}_{\text{eff}} + \alpha \mathbf{M} \times \frac{d\mathbf{M}}{dt}, \tag{1}$$

where $\mathbf{M}$ is the magnetization vector, $\mathbf{H}_{\text{eff}}$ is the effective magnetic field acting on the magnetization, γ is the gyromagnetic ratio and α is the Gilbert damping parameter. The term $-\gamma \mathbf{M} \times \mathbf{H}_{\text{eff}}$ is recognized as the precessional component, influencing the rotational behavior of the magnetic moment relative to the effective magnetic field $\mathbf{H}_{\text{eff}}$. Conversely, the expression $\alpha \mathbf{M} \times \frac{d\mathbf{M}}{dt}$ contributes to damping, regulating the gradual loss of energy in the magnetic moment's motion over time.

Magnetization, denoted as $\mathbf{M}$, encapsulates the density of magnetic moments within a material. The effective magnetic field, $\mathbf{H}_{\text{eff}}$, integrates the external magnetic field with internal influences, including anisotropy and the exchange interaction. The gyromagnetic ratio, γ, characterizes the link between a particle's magnetic moment and its angular momentum. Lastly, the Gilbert damping parameter, α, modulates the damping force's intensity, which affects how swiftly the magnetization realigns with $\mathbf{H}_{\text{eff}}$ [18].

A quantitative analysis of the oscillation frequency (f) as a function of H_{ext} can be used to extract the magnetization dynamics parameters of the device [17]. We assume that our data is well described by the ferromagnetic resonance mode obtained from the LLG equation with $\alpha << 1$ and assuming a thin film and in plane magnetic field,

$$f = \frac{g\mu_B\mu_0}{2\pi\hbar}\sqrt{|H_{eff}|(|H_{eff}| - H_{int}\sin^2(\theta_M))}, \tag{2}$$

which introduces, g = 1.89 as the Lande g-factor, μ_B the Bohr magneton, $H_{eff} = H_{ext} + H_{int}\cos(\theta_M)\,\hat{Z}$, with $H_{int} = \frac{2K}{\mu_0 M_s} - M_s$. Here, M_s the saturation magnetization, and θ_M the angle between M and the magnetic sample normal (z-direction). The angle θ_M is calculated by minimizing the magnetic energy in the presence of an external field, perpendicular magnetic anisotropy, and shape anisotropy.

2.5 Magnetization dynamics parameters

2.5.1 Applying external Magnetic field

When an external magnetic field is applied to a material, the magnetic moments align with the field direction, minimizing the system's energy through Zeeman energy [5]. The degree and manner of alignment depend on the strength and orientation of the applied field, the material's magnetic properties, and the temperature.

The Kittel formula provides the conditions for ferromagnetic resonance (FMR), differentiating between parallel and perpendicular external magnetic fields relative to the thin film's plane [19]. For the parallel configuration, the formula is

$$f = \frac{\gamma}{2\pi}\sqrt{H_{\text{eff}}(H_{\text{eff}} + M_s)}\ , \tag{3}$$

This configuration elucidates the combined effects of anisotropy and magnetization on the resonance frequency. In contrast, the perpendicular configuration is described by

$$f = \frac{\gamma}{2\pi}(H_{\perp} - M_{\text{s}}), \tag{4}$$

where $H_{\perp}$ is an external magnetic field, applied out of plane with respect to the thin film. This highlights the direct influence of the external field and effective magnetization on the resonance frequency. The parallel configuration emphasizes the role of internal magnetic properties (anisotropy and effective magnetization) in determining the resonance condition, while the perpendicular setup focuses on the external field's modulation of the resonance, making each configuration suited for probing different aspects of magnetic materials.

2.5.2 Anisotropy

Magnetic anisotropy refers to the dependence of a material's magnetic properties on the direction of magnetization [20]. There are two primary types of magnetic anisotropy: Shape and crystalline. Both shape anisotropy and crystalline anisotropy contribute to the overall magnetic behavior of materials, influencing their magnetic properties and applications in various technologies [21].

The influence of anisotropies can be likened to the effect of an extra applied magnetic field; thus, it is possible to approach it in this manner. Generally, one can calculate an anisotropy field from the anisotropy energy by using the formula [18]

$$\vec{H} = -\frac{1}{|M|}\nabla E_{\text{anis}}(\vec{M}), \tag{5}$$

a) **Shape anisotropy**

This type of anisotropy arises from the shape of a magnetic material. When a magnetic material has a particular shape, such as a thin film or a particle, the arrangement of its magnetic moments tends to align preferentially along a specific axis. The geometry of the material influences the energy associated with the alignment of magnetic moments, leading to a preferred orientation or easy axis for magnetization [21].

Shape anisotropy originates from the minimization of magneto static energy associated with stray fields, also known as demagnetization fields, are magnetic fields that extend outside the physical boundaries of a magnetic material, they are influenced by the material's geometry.

For instance, in thin films, magnetic moments align within the plane to minimize the stray fields' extension beyond the material, reducing magneto static energy. Conversely, elongated particles favor magnetization along their long axis, decreasing the surface area affected by stray fields and thus the energy cost. This directional preference for magnetization, dictated by the material's shape, minimizes the overall energy of the system by reducing the impact of stray magnetic fields, leading to a preferred orientation or easy axis for magnetization [22]. The shape anisotropy field can be expressed as

$$\vec{H}_{shape} = -\overline{\overline{N}}\vec{M}, \tag{6}$$

Where $\overline{\overline{N}} = \sum N_{ij}\hat{i}\hat{j}$ is the demagnetization tensor $(i, j \in x, y, z)$. Assuming we can obtain the precession frequency of the magnetization in a sample dominated by shape anisotropy. Assuming a ferromagnetic thin film, equation 6 can be utilized to get another version of the Kittel formula which involves the demagnetization factors due to the shape anisotropy, resulting formula for precession frequency is [18]

$$f = \frac{\gamma\mu_0}{2\pi}\sqrt{[(N_z - N_x)M_s + H_x^{DC}][(N_y - N_x)M_s + H_x^{DC}]}, \tag{7}$$

b) **Crystalline anisotropy**

Crystalline anisotropy is inherent to the crystal structure of a material. The arrangement of atoms in the crystal lattice can create preferential directions for magnetization. Different crystallographic axes may have different magnetic properties, and the energy associated with aligning the magnetic moments along these axes can vary. This type of anisotropy is particularly relevant in crystalline magnetic materials, where the crystal symmetry determines the preferred direction for magnetic alignment [21].

For example, Iron's magnetic characteristics are intricately linked to its crystal structure, with the orientation of its magnetic moments relative to the crystal axes playing a crucial role. Magnetic moments align most readily along certain crystallographic directions, known as the easy axis, due to a lower energy requirement. Some crystallographic directions are more energetically favorable due to the way unpaired electrons align and interact with each other within a material's atomic structure [23].

The uniaxial anisptropy constant is represented by K , seen in equation 2.Quantifying the energy required to change the orientation of magnetic moments or structural elements along a preferred axis in a crystal lattice. In the context of magnetic materials, K influences the stability of magnetic domains, dictating the ease with which the magnetic moments align parallel or anti parallel to the designated axis. Higher values of K indicate stronger uniaxial anisotropy, making it more challenging to alter the material's magnetic alignment [21].

2.5.3 Exchange stiffness

Exchange stiffness, a fundamental parameter in the physics of magnetic materials, quantifies the resistance of the magnetic moments (or spins) within a material to being reoriented relative to each other. It is a strength measurement of the exchange interaction, the quantum mechanical phenomenon that causes spins to align parallel or anti parallel to each other, depending on whether the interaction is ferromagnetic or antiferromagnetic, respectively [24].

The exchange stiffness, denoted by A, is used in several key equations in magnetism, including the micro magnetic model which describes the energy of a magnetic system. One of the most

relevant expressions where A appears is in the formula for the exchange energy density, given by:

$$E_{\text{exchange}} = A\left(\nabla \mathbf{m}\right)^2, \tag{8}$$

where $\mathbf{m}$ is the unit vector in the direction of magnetization, and $\nabla \mathbf{m}$ represents the spatial gradient of $\mathbf{m}$. The unit of exchange stiffness is typically joules per meter (J/m), highlighting its role as a measure of the energy required to change the spatial orientation of magnetization over a certain distance [25]. This directly effects M and H_{eff} and thus prevalent in the LLG equation. Moreover, the exchange stiffness constant is

$$A_{\text{ex}} = S^2 \frac{J_{\text{ex}}}{a}, \tag{9}$$

with spin denoted as S, and J_{ex} is the exchange energy, which tends to align the electron spins/magnetic moments parallel to each other, creating homogeneity in the magnetic sample. While, a is the atomic distance [26].

Physically, exchange stiffness is a measure of the strength of the coupling between neighboring magnetic moments. A high value of A indicates strong coupling, making it difficult for the orientations of the magnetic moments to diverge from each other. This strong coupling ensures that the magnetic moments tend to align uniformly, maintaining coherence over larger distances within the material. The exchange stiffness is crucial for the frequency precision of magnetic moments precessing around an external magnetic field. In the context of frequency precision, a higher exchange stiffness means that the magnetic moments are more tightly bound to each other's orientation, leading to a more coherent and uniform precession across the material. This uniformity is essential for applications requiring high frequency precision, such as in spintronics and magnetic resonance technologies, where the precise control and manipulation of spin dynamics are critical.

2.5.4 Damping

Damping denoted as α in the LLG equation, refers to the dissipation of energy in a magnetic system, particularly the loss of energy associated with the motion of magnetic moments. It plays a crucial role in determining the dynamics of magnetization, influencing phenomena such as the precession of spins and the propagation of spin waves [27].

In the presence of an external magnetic field, the precession of spins—often associated with the phenomenon of Larmor precession—can be subject to damping effects . Damping introduces a decay in the amplitude of the precession motion over time, leading to the relaxation of the magnetic system toward equilibrium. Mumax3 (explained in section 2.6) can be utilized to model this phenomena.

2.5.5 Magnetic exchange length

In micro magnetic modeling, the exchange length (l_{ex}) is a foundational concept that establishes the critical dimension over which the exchange interactions dominate magneto static influences. Represented mathematically as [28]

$$l_{\text{ex}} = \sqrt{\frac{A_{\text{ex}}}{K_m}}, K_m = \frac{1}{2}\mu_0 M_s^2, \tag{10}$$

where A_{ex} stands for the exchange stiffness and M_S is the saturation magnetization. The exchange length informs the minimum scale necessary for accurate simulations of magnetic

behavior, particularly in soft magnetic materials where domain walls predominantly contain volume charges.

2.6 MuMax3

MuMax3 is a state-of-the-art open-source software package designed for performing micro magnetic simulations, particularly focusing on the dynamics and behavior of magnetic moments within materials [29]. MuMax3 is extensively employed for simulating and analyzing the behavior of magnetic moments in diverse materials, providing insights into the magnetic properties of systems at the nano-scale, this is done through solving the LLG equation. Its applications range from investigating magnetic domain dynamics to studying the response of magnetic materials under different external conditions.

The software is particularly advantageous for simulating magnetic moments in samples with specific properties and geometries. Users can define the material characteristics, such as anisotropy, exchange interactions, and damping coefficients, to accurately represent the physical properties of the simulated magnetic samples. Additionally, the geometry of the samples can be customized, allowing for the study of thin films or multilayered structures. MuMax3 facilitates the application of external magnetic fields to the simulated systems, enabling the exploration of how varying field strengths and orientations influence the magnetic behavior of the samples. This capability is essential for understanding how magnetic moments respond to external stimuli, contributing to the broader field of magnetic materials research.

3 Method

In our study, we embarked on a comprehensive simulation to study the intricate dynamics of magnetization in varying geometries and physical conditions. The basis code is in section 9.2.1 from which all parameters are changed. Furthermore, MuMax3 generates Output Vector Field (OVF) files that capture the spatial distribution of magnetic moments and associated parameters throughout the simulated structures. OVF files are then analysed through the python code in section 9.3.1. The code processes magnetic moment values from each column, averages them by file (time point), and appends them to lists for mx, my, and mz. Frequency is then determined using FFT on these lists, validated through visual comparison.

Initially, our focus was on a cubic magnetic sample to investigate the influence of shape anisotropy and the exchange length and stiffness on the magnetization dynamics. This involved simulations across a spectrum of magnetic fields, both in the presence and absence of periodic boundary conditions (PBC). The choice of zero field aimed at isolating the effects of shape anisotropy. For the exchange stiffness, explored values are $A_{ex} = 10^{-10}$ J/m and 10^{-12} J/m. Moreover, for the exchange length here the grid size was changed to explore if there are any frequency changes, done through changing *SetGridsize* values. Moreover, when *PBC* was set to (2,2,2) to maintain an equal shape anisotropy. This effectively eliminates edge effects and artificial interactions at the boundaries, ensuring that the magnetic behavior within the modeled sample is representative of the actual physical system.

The exploration extended to the simulation of a thin film magnetic sample, adhering to the assumptions of the Kittel formula. This phase of the simulation varied the sample sizes while maintaining a constant ratio between length and height, finding it by looking at different ratios and investigating their precissional frequency in order to find the optimal exchange length. Alongside adjustments in the exchange stiffness constants (A_{ex}) to gauge their impact on the sample's homogeneity. Utilizing the advanced capabilities of MuMax3, the simulations were converted into 3D visualizations via mumax-view, visualizing the orientation of the magnetic moments in the sample as colored arrows, where different colors represent different orientation thus helping the visualization when zoomed out.

Diving deeper, the investigation into the thin film sample was further enriched by altering the magnetic field strengths, including the scenario of zero magnetic field to accentuate the shape anisotropy effects. This meticulous analysis was carried out under varying conditions of magnetic anisotropy constant (K), exploring values of $K_0 = 0$ J/m^3, $K_1 = 0.345 \cdot 10^5$ J/m^3, chosen from [30] and $K_2 = 2 \cdot K_1 = 0.69 \cdot 10^5$ J/m^3, to understand the uniaxial anisotropy's impact on the magnetic order within the sample. K_2 is chosen to be twice as K_1 to have a measurable impact on the oscillation frequencies of the magnetic moments in the sample. *PBC* was set to (1,1,0) maintaining same shape anisotropy and eliminating edge effects. Furthermore, after investigating two samples with different anisotropies separately, it is time to put them next to each other, and examine the precissional frequencies. The magnetic sample length is to remain constant while the first half are set to K_1 while the second half is K_2. Mumax3 script shown in section 9.2.2.

The oscillation frequency (f) of the sample's macrospin can be calculated in two different way. Firstly, as it was previously measured, where the entire sample's magnetic moments vectors are averaged in every file (so each time point) then looking at the frequency using the FFT python function. Contrary, examining each half frequency on its own. This is done by only looking at each half (each with different anisotropy) then calculating the precessional frequency, code seen in the section 9.3.2. This allows us to measure f for each half with a different anisotropy constant.

4 Results

4.1 Initial simulations

First, a simulation of a cuboid magnetic sample was created in order to study how the magnetic moments in it behaves with various magnetic fields. The sample has dimensions of 500x10x50 cells while each cell is 1 nm in size. The geometry is visualized in Figure 4 and the magnetic moments are all initialised in the x-direction.

It was anticipated that applying both the external magnetic field (B = 0.1 T) and uniaxial anisotropy ($K = 0.34 \cdot 10^5\ J/m^3$) in the z-direction would produce a specific outcome: two out-of-phase, decaying sinusoidal waves with constant frequencies for $< m_x >$ and $< m_y >$ (average magnetic moment in x and y direction respectively), along with an increase of $< m_z >$ to 1, reflecting the orientation of the B and K fields. However, as Figure 3 demonstrates, the actual results diverged from these expectations. This deviation is attributed to the influence of shape anisotropy, an overlooked factor that exerts an additional force on each magnetic moment, leading to the observed discrepancy. Where the decaying waves are irregular with non-constant frequencies. Meanwhile, around 0.4-0.5 ns a regular oscillation of m_y and m_x is seen and by 1 ns the amplitude of m_y is shown to decrease, indicating damping.

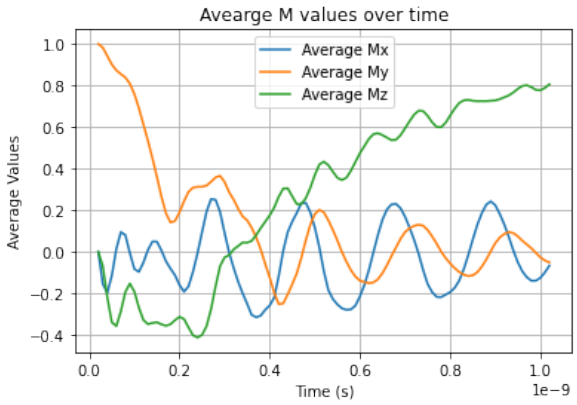

Figure 3: Magnetic sample with dimensions (500x10x50) with an initial magnetic moment in x-direction, and apply an external magnetic field (0,0,0.1 T). The figure shows the average magnetic moments' evolution over time.

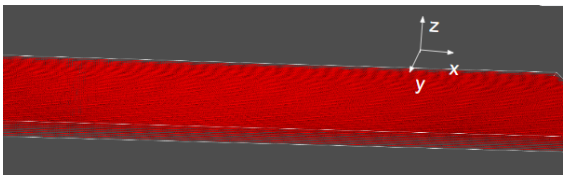

Figure 4: 3D visualization of a magnetic sample, with dimensions of 500 nm x 10 nm x 50 nm. Done through mumax-view [31]

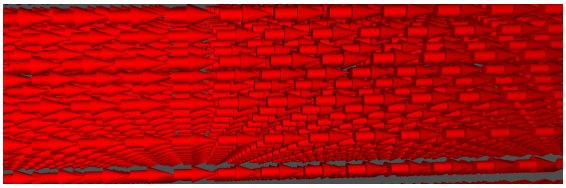

Figure 5: Cuboid magnetic sample, zoomed in. The red arrows are in the x-direction, each indicating a magnetic moment with dimensions of 1 nm,1 nm, 1 nm.

4.2 Cubic magnetic sample

4.2.1 Anisotropy and Kittel formula

A cubic magnetic sample was made in order to avoid the shape anisotroy, with sides of 50 nm, visualised in Figure 6. To see this, a simulation was ran yet with B = K = 0. As expected, every magnetic moment stayed stationary in every direction over time.

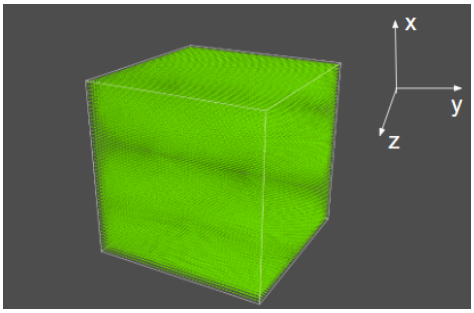

Figure 6: Visualization of a 3D cube, filled with magnetic moments. Green indicates they are pointing the y-direction.

Additionally, the external magnetic field was increased in increments of 0.1 T to 0.6 T in the y-direction. Note that due to the shape, the field direction does not matter as long as it is not the same as the initialized magnetic moment, assuming $K = 0$ or in the same direction as B. Fore each magnetic field the precissional frequency was estimates using the FFT function as shown in the python code in section 9.3.1. As seen in Figure 7 the first frequency coincides with the Kittel formula, however, the gap between the Kittel formula frequencies and cube frequencies increases with the magnetic field. Note that only frequency of m_x was plotted, since it is the same as the others. This does not match the Kittel formula, since in the Kittel formula's derivation, the shape is assumed to be a thin film. Hence, a thin film should be simulated and compare their results with the theory from Kittel formula. In a cubic sample, the magnetic moments can align more freely along different crystallographic directions, leading to a higher precessional frequency. In contrast, thin films have a preferred magnetization directions due to shape anisotropy and surface effects, limiting the freedom of magnetic moment alignment and resulting in a lower precessional frequency.

Figure 8: Visualizing the cubic magnetic sample at t = 1 ns for (a) $A_{\text{ex}} = 10^{-12}$ J/m, and (b) $A_{\text{ex}} = 10^{-10}$ J/m. Where, colors represent different moment directions as seen through Figure 15.

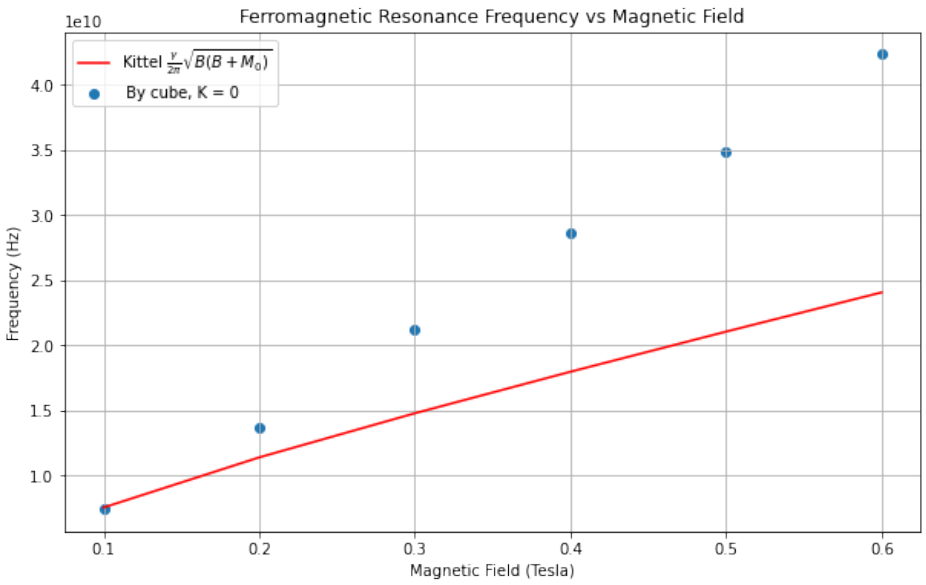

Figure 7: Investigating m_x, m_y precissional frequencies around increasing magnetic field, with $K = 0$. For a cubic magnetic sample. The blue dots represent the extracted frequencies using the FFT function ,seen in the python code in section 9.3.1, of the Mumax3 simulation. While, the red line is the theoretical frequency values using the Kittel formula, equation 2.

4.2.2 Exchange stiffness

In order to gain a deeper understanding of the magnetic moments evolution, a feature in Mumax3 was utilized to convert each file (point in time) to a 2D image. Figure 8.a shows the cube magnetic moments at t = 1 ns, the figure illustrates the in-homogeneity of the magnetic sample over time with $A_{\text{ex}} = 10^{-12}$ J/m . This phenomenon is attributed to the exchange stiffness: an increase in this parameter enhances the interaction between magnetic moments, promoting homogeneity, as illustrated in Figure 8.b, where $A_{\text{ex}} = 10^{-10}$ J/m.

4.3 Thin film

4.3.1 Grid size and exchange stiffness

A thin film is created through grid dimensions of 40x40x10, visualized in Figure 9.

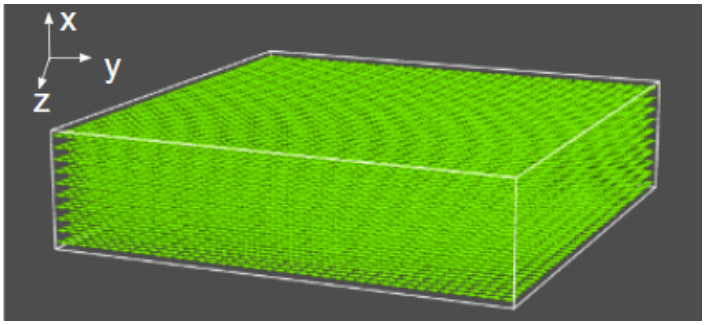

Figure 9: 3D visualization of the thin film/cuboid with magnetic moments initialized in the y-direction, indicated through the green arrows.

The frequency is influenced through both the grid size and the exchange stiffness. However, these parameters are computationally expensive to increase, thus a series of simulation was ran to see the most optimal parameters. Moreover, a series of simulations was also done to examine which factor between the length and height produces a frequency closest to the theoretical frequency from Kittel, this is examining the exchange length. The found ratio was 4, where after the frequency stayed constant. Aspect ratio is defined here to be the ratio between the length, and height of the sample, where *SetGridSize* has variables of (Length,Width,Height). Meanwhile, the width is set to be equal to the length to have equal shape anisotropies in the x and y direction. Hence from question 7, $N_x = N_y = 1, N_z = 0$.

Through the results summarized in Table 4.3.1 it can be seen that the measured frequency is close to the theoretical model from Kittel when either the grid size increases (yet the ratio of 4 stays the same) or the exchange stiffness increases. However, increasing both does not decrease the difference between the simulated and the theory. The exchange stiffness was chosen to be increased to $A_{\text{ex}} = 10^{-10}$ J/m, since increasing the size is more computationally heavy.

Grid Size [x,y,z] (nm)	$A_{\text{ex}}(J/m)$	f(GHz)	$l_{\text{ex}}(nm)$
$[200, 200, 50]$	10^{-12}	6.93	2.5
$[40, 40, 10]$	10^{-12}	5.88	2.5
$[40, 40, 10]$	10^{-10}	6.93	25
$[40, 40, 10]$	10^{-10}	6.93	25
$[200, 200, 50]$	10^{-10}	6.93	25
$[4, 4, 1]$	10^{-10}	6.93	25

Table 1: Summary of *SetGridsize*, exchange stiffness (A_{ex}) and length configurations and results. In each simulation, $m = (1, 0, 0)$, $B = (0, 0.1, 0)$, where frequency obtained from Kittel equation is $f_{\text{kittel}} = 7.5$ GHz.

4.3.2 K_0

After optimising the grid size, dimensions, exchange stiffness and external magnetic field direction with respect to the magnetic moments, thin film is simulated with different B field

values and we measure each precissional frequency. Here we apply no uniaxial anisotropy, $K_0 = 0\ J/m^3$. It is seen from Figure 10 that the simulation is closer to the theoretical model, using Equation 2, than the cube as. This is expected since the Kittel formula is based on thin films. Moreover, both γ and M_s where fitted and found to be $M_{s,\text{fit}} = (451.58 \pm 0.001) \cdot 10^3$ A/m^3 and $\gamma_{fit} = (1.6127 \pm 0.0001) \cdot 10^{11}$ MHz/T , while the actual values are $500 \cdot 10^3$ A/m^3 and $1.76 \cdot 10^{11}$ MHz/T respectively. The difference between the measured M_s and the inputted value arises from shape anisotropy. While the Kittel formula considers only M_s, it doesn't account for the effective saturation magnetization (M_{eff}), which incorporates shape anisotropy. Therefore, the measured value is not M_s, but rather M_{eff}.

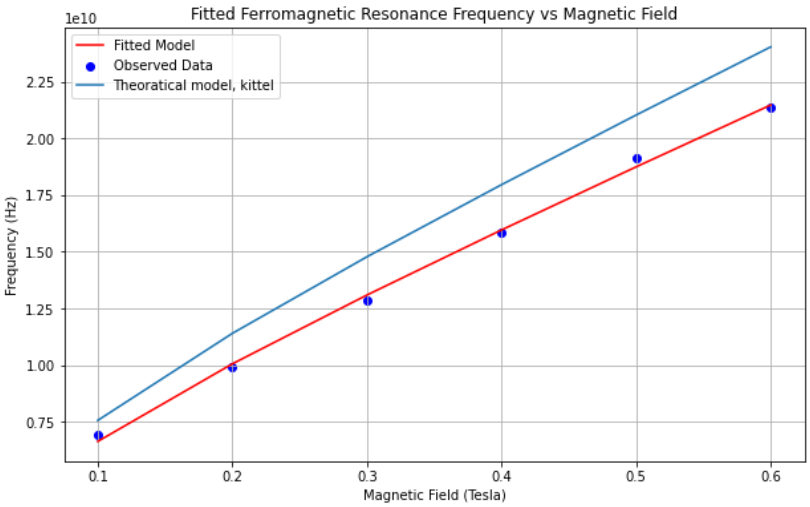

Figure 10: Investigating m_x, m_y precissional frequency around increasing magnetic field. For a magnetic sample, with a geometry of a thin film and no anisotropy. This is for K = 0.

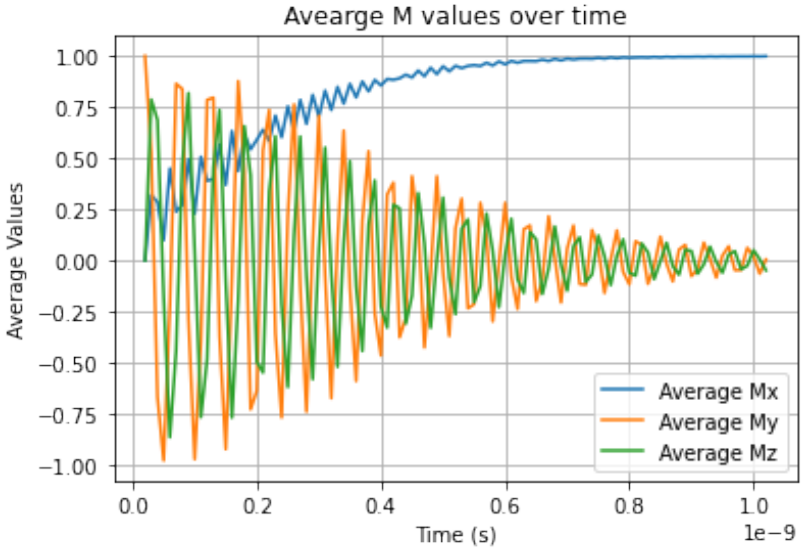

Figure 11: Average magnetic moments in x,y,z directions over time, with an applied field of 0.5 T $\hat{x}$, K = 0 and m = (0,1,0)

4.3.3 K_1, K_2

In addition, instead of $K = 0\ J/m^3\hat{\mathrm{x}}$, two different constants are set. The values are $K_1 = 0.345 \cdot 10^3\ J/m^3\hat{\mathrm{x}}$ and $K_2 = 2 \cdot K_1\ J/m^3\hat{\mathrm{x}}$. As seen from Figure 12, data shows an increase in precessional frequency with an increase in uniaxial anisotropy and magnetic field, note that f values for K_2 are consistently higher than K_1. This is predicted from the Kittel formula, where an increase in anistropy causes an increase in the effective field and thus a higher precissional frequency value.

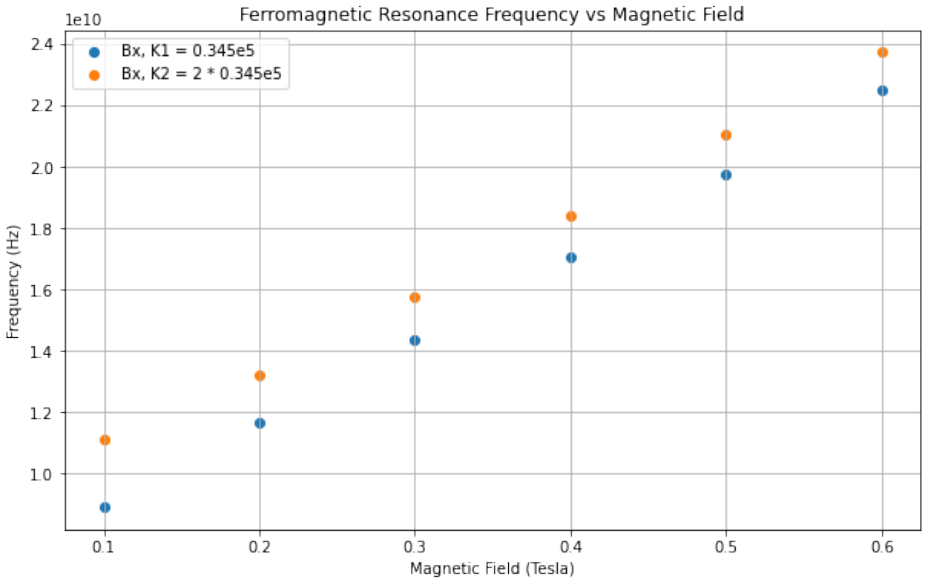

Figure 12: Investigating m_x, m_y precissional frequency around increasing magnetic field. For a magnetic sample, with a geometry of a thin film with grid size of 40x40x10 cells, 1 nm each. For $K_1 = 0.345 \cdot 10^5\ J/m^3\hat{\mathrm{x}}$, $K_2 = 2 \cdot K_1\ J/m^3\hat{\mathrm{x}}$.

4.4 Two domains

Finally, the magnetic sample is split into two connected parts, visualized in Figure 13. Each part has a separate anisotropy of K_1, K_2. The size and geometry of the sample is still the same as the previous simulations with one anisotropy constant, however, using the Mumax3 script in section 9.2.2 we set the first 20 cells with K_1 and second 20 cells with K_2. This represents if two different samples with different anisotropy constants would be stacked next to each other in the x-direction. Which represents the initial goal of having a magnetic crystal of alternating magnetic anisotropy constants as seen in Figure 1. Done through electrostatic gating, where you have an alternating voltage gates of V_1 and V_2, creating samples of K_1 and K_2. The simulation is run with m = (0,1,0) and the anisotropies and magnetic field are both applied in the x-direction.

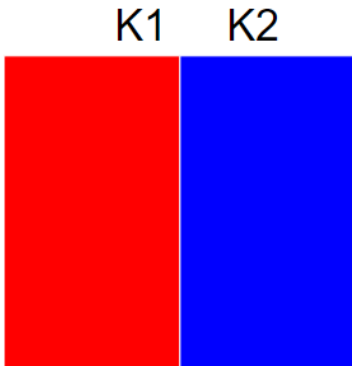

Figure 13: Visualization of two domain magnetic sample, with two connected parts with different anisotropies, K_1, K_2.

As seen through Figure 14 both domains have the same frequency and wave pattern in every magnetic moment direction. The calculation is performed to evaluate the precessional frequency of magnetic moments in each half of the sample separately using the python script in section 9.3.2. Moreover, when the total average frequency is taken as before through script in 9.3.1, for the whole sample, the frequency is still approximately the same as measuring it in each sample separately. This shows that the macrospin of each part has an equal precessional frequency to the macrospin of the total sample. Indicating a homogeneous macrospin throughout the entire sample, which is due to the high exchange stiffness ($A_{\text{ex}} = 10^{-10}$ J/m) hence exchange length ($l_{\text{ex}} = 25\ nm$) values. In addition, increasing the ratio, $\frac{K_2}{K_1}$ lead to an approximate increase in frequency by 0.5 GHz.

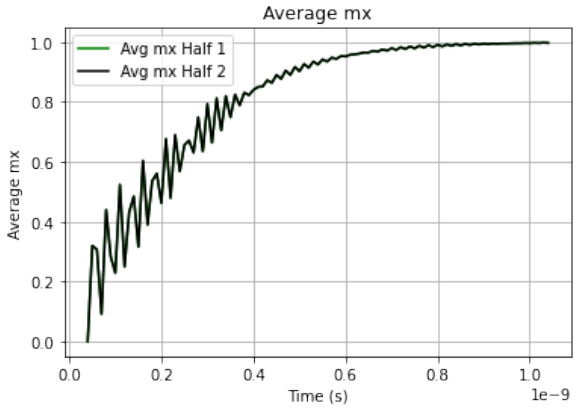

(a)

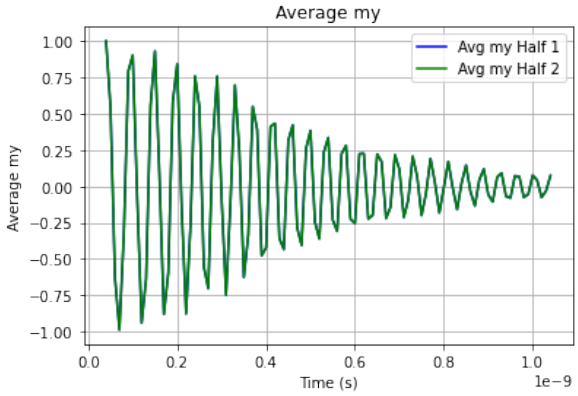

(b)

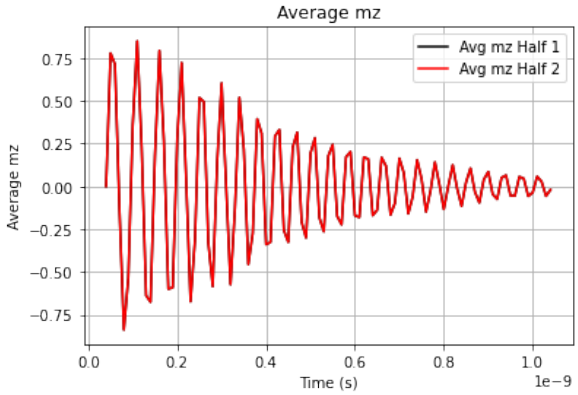

(c)

Figure 14: Average magnetic moments over time, for both parts of the sample. (a) magnetic moment in x-direction over time, while (b) is the y-direction and (c) is the z-direction. Done for B = 0.3 T $\hat{x}$ and $K_1 = 0.345 \cdot 10^5$ $J/m^3\hat{x}$, $K_2 = 2 \cdot K_1$ $J/m^3\hat{x}$. Where both 1st and 2nd part average magnetic moments overlap for all directions.

5 Discussion

The behavior of magnetic moments and their precissional frequencies were investigated, in each direction, while varying the magnetic field strength and direction, and the anisotropy constant value. Moreover, investigating these frequencies with different sample parameters such as the exchange length, aspect ratio and grid size. Optimizing these parameters to get closer to the theoretical model with the least computational power. In the simulation, the sample dimensions were set to 500x10x50 cells, where each cell is 1 nm, emphasizing shape anisotropy predominantly in the x-direction due to it being the largest axis. Moreover, as seen in Figure 5, the magnetic moments are initialized in the x-direction. It was found through simulating a magnetic cube sample, that exchange length needs to be increased through increasing the exchange stiffness constant in the Mumax3 script, in order to maintain homogeneity.

A thin film with dimensions of 40x40x10, was explored. The film's initial magnetic moments were oriented in the y-direction, and simulations were conducted across varying strengths of in-plane magnetic fields in the x-direction. Three distinct uniaxial anisotropies were tested, all of which yielded results within the range predicted by the Kittel formula, as depicted in Figures 10 and 12. For $K_0 = 0$, the simulation-derived frequencies were matched to the Kittel formula (Equation 2) using fitted values for M_s and γ. The fitted γ_{fit} closely approximates the input value, but the M_s is higher than the fitted $M_{s,\text{fit}}$. This discrepancy arises from shape anisotropy, as the Kittel formula considers M_s rather than M_{eff}, which is influenced by shape anisotropy. The error percentage calculated through the discrepancy between M_s and $M_{s,\text{fit}}$ is 10%. In addition, Figure 12 shows that since that the effective field is increased through the anisptropy constant, just like increasing the magnetic field it creates a faster oscillation frequency.

The primary objective was to simulate a magnetic crystal with a variable anisotropy constant. The study revealed consistent precessional frequencies and wave patterns across two distinct domains within the magnetic sample, as illustrated in Figure 14. Utilizing Python scripts for calculations, it was found that the frequencies of individual domains closely aligned with the average frequency of the entire sample. This uniformity indicates a homogeneous macrospin across the sample, which can be attributed to high exchange stiffness ($A_{\text{ex}} = 10^{-10}$ J/m) and exchange length ($l_{\text{ex}} = 25$ nm) values. An increase in the ratio $\frac{K_2}{K_1}$ increased the frequency by $0.5GHz$.

An error lies in Mumax3, the exchange length and the grid size were all optimised with respect to each other to minimize computational time and power. Since, when it took too long the terminal terminated the job. Increasing the exchange length and stiffness leads to more accurate results. On the other hand, these simulations might be unnecessary since in practice these dimensions simulated are realistic.

Future research could explore the simulation further, focusing on a magnetic sample composed of two distinct parts with different uniaxial anisotropies. Additional simulations could examine how the exchange length affects this setup. As the exchange length decreases, each part's frequency is expected to become more distinct due to reduced magnetic moment interactions, leading to less homogeneity. Increasing the ratio between the sample's anisotropies elevates the overall frequency. An intriguing approach would be to vary K_2 by n and K_1 by $1/n$, progressively increasing n to maintain a consistent ratio while amplifying the anisotropy difference. Furthermore, Applying an out-of-plane effective field, could be performed. Equation 3 could be fitted to the resulting values for both the single and dual uniaxial anisotropy samples to analyze separate and overall oscillation frequencies.

6 Conclusion

In conclusion, the initial simulations in section 4.1 revealed an unusual trend attributed to the experimental setup, particularly due to the shape anisotropy being largest in the x-direction and the application of the magnetic field and uniaxial anisotropy in the z-direction, not aligning with the Kittel formula's assumptions. Adjustments to parameters such as exchange stiffness and aspect ratio (length/height) were explored to understand their effects on precessional frequency, finding that increasing exchange stiffness is necessary for maintaining homogeneity, and an aspect ratio of 4 is sufficient for thin films. Despite achieving results within the Kittel formula range, notable errors were identified, primarily due to constraints within Mumax3 for computational efficiency. These findings suggest that simulations can closely replicate theoretical predictions with an error of 10%, which is calculated through the discrepancy between M_s and $M_{s,\text{fit}}$. However, practical experiments may still diverge due to inherent experimental variables. The study successfully simulated a magnetic crystal with a variable anisotropy constant, revealing consistent precessional frequencies across two domains, indicative of a homogeneous macrospin. This uniformity was attributed to high exchange stiffness and length values, with frequency increasing proportionally to the ratio of anisotropy constants. In future research on the two-domain sample, it would be valuable to explore the impact of varying exchange length on individual domain frequencies and to examine the effects of anisotropy differences while maintaining a constant ratio. Additionally, investigating the influence of an out-of-plane external magnetic field on thin films with both single and dual domains, and comparing the results with theoretical predictions from Equation 3, could provide further insights.

7 Acknowledgments

Firstly, I would like to thank the research group of Opto-Spintronics of Quantum Materials for giving me the opportunity to work with them, they were very welcoming. It was a great opportunity to work under M.H. Guimaraes, who have helped me weekly and taught me how to think and research better. For which I will always be grateful. Furthermore, I would like to thank my daily supervisor Rixt Boxma for all her help and patience with me. Her constant feedback and help got me through this thesis.

8 References

[1] The Editors of Encyclopaedia Britannica. magnon. Jun 2020. Accessed 22 February 2024.

[2] Zhihao Jiang, Jinho Lim, Yi Li, Wolfgang Pfaff, Tzu-Hsiang Lo, Jiangchao Qian, André Schleife, Jian-Min Zuo, Valentine Novosad, and Axel Hoffmann. Integrating magnons for quantum information. *Applied Physics Letters*, 123(13):130501, 09 2023.

[3] Alison Roxburgh and Ezio Iacocca. Nano-magnonic crystals by periodic modulation of magnetic parameters. *Magnetochemistry*, 10(3), 2024.

[4] J R Schrieffer. What is a quasi-particle? *Journal of Research of the National Bureau of Standards. Section A, Physics and Chemistry*, 74A(4):537–541, 1970.

[5] Charles Kittel. *Introduction to Solid State Physics*. Wiley, 8 edition, 2005.

[6] AG Demokritov. What are spin waves? https://www.uni-muenster.de/Physik.AP/Demokritov/en/Forschen/Forschungsschwerpunkte/mBECwasw.html, Access Year. Accessed: 05/02/2024.

[7] Quantum Science and Engineering at University of Delaware. Magnonic materials for quantum device applications. https://qse.udel.edu/research/magnonic-materials-for-quantum-device-applications/, 2022. Accessed: 07/03/2024.

[8] V V Kruglyak, S O Demokritov, and D Grundler. Magnonics. *Journal of Physics D: Applied Physics*, 43(26):260301, 2010.

[9] S. A. Wolf, A. Y. Chtchelkanova, and D. M. Treger. Spintronics—a retrospective and perspective. *IBM Journal of Research and Development*, 50(1):101–110, 2006.

[10] Jianyu Zhang, Mingfeng Chen, Jilei Chen, Kei Yamamoto, Hanchen Wang, Mohammad Hamdi, Yuanwei Sun, Kai Wagner, Wenqing He, Yu Zhang, Ji Ma, Peng Gao, Xiufeng Han, Dapeng Yu, Patrick Maletinsky, Jean-Philippe Ansermet, Sadamichi Maekawa, Dirk Grundler, Ce-Wen Nan, and Haiming Yu. Long decay length of magnon-polarons in bifeo3/la0.67sr0.33mno3 heterostructures. *Nature Communications*, 12(7258):1–8, 2021.

[11] Arabinda Haldar and Adekunle Olusola Adeyeye. Functional magnetic waveguides for magnonics. *Applied Physics Letters*, 119(6), 2021.

[12] Michael Balinskiy and Alexander Khitun. Yttrium iron garnet-based combinatorial logic and memory devices. *IEEE Journal on Exploratory Solid-State Computational Devices and Circuits*, page 99, 2022.

[13] H.Y. Yuan, Yunshan Cao, Akashdeep Kamra, Rembert A. Duine, and Peng Yan. Quantum magnonics: When magnon spintronics meets quantum information science. *Physics Reports*, 965:1–74, 2022. Quantum magnonics: When magnon spintronics meets quantum information science.

[14] Ella O. Lachman, Rafael Haenel, Daniele Pinna, Felix Casola, Amir Yacoby, Christian H. Back, and Geoffrey S. D. Beach. Electrostatic gating of magnons via superconducting proximity effect. *Physical Review Letters*, 129:117201, 2023.

[15] San-Dong Guo, Xiao-Shu Guo, Guang-Zhao Wang, Kai Cheng, and Yee-Sin Ang. Electric-field induced magnetic-anisotropy transformation to achieve spontaneous valley polarization. *J. Mater. Chem. C*, 10:16363–16369, 2022.

[16] Michael Schirber. Voltage control over magnons, 2024.

[17] Freddie Hendriks, Rafael R. Rojas-Lopez, Bert Koopmans, and Marcos H. D. Guimarães. Electric control of optically-induced magnetization dynamics in a van der waals ferromagnetic semiconductor. *arXiv*, 2309.12776v1, September 2023. [cond-mat.mes-hall].

[18] Csaba Józsa. *Optical detection of the magnetization precession: Choreography on a sub-nanosecond timescale*. Phd thesis, Technische Universiteit Eindhoven, 2006.

[19] Zhuangqu Zhang and Yajun Wei. Optimization of experiment settings in ferromagnetic resonance measurements. *Results in Physics*, 7:2614–2618, 2017.

[20] ScienceDirect. Magnetic anisotropy. https://www.sciencedirect.com/topics/chemistry/magnetic-anisotropy, 2024. Accessed: 2024-03-07.

[21] Institute for Rock Magnetism, University of Minnesota. 3 magnetic anisotropy. https://cse.umn.edu/irm/3-magnetic-anisotropy.

[22] Department of Materials Science and Metallurgy University of Cambridge. Dissemination of it for the promotion of materials science (doitpoms).

[23] Chemistry LibreTexts. 14.2: Magnetic properties of materials. https://chem.libretexts.org/, 2023.

[24] JH Shim, AA Syed, Y Shin, et al. Ultrafast dynamics of exchange stiffness in co/pt multilayer. *Communications Physics*, 3:74, 2020.

[25] M. D. Kuz'Min, K. P. Skokov, L. V. B. Diop, I. A. Radulov, and O. Gutfleisch. Exchange stiffness of ferromagnets. *The European Physical Journal Plus*, 135(3), 2020. HAL Id: hal-02920032.

[26] Umesh K.Mishara and Jasprit Singh. *Semiconductor Device Physics and Design*. Springer, 2008.

[27] W. M. Saslow. Landau–lifshitz or gilbert damping? that is the question. *Journal of Applied Physics*, 105(7):07D315, 2009.

[28] Felipe Garcia-Sanchez. Dynamics of magnetic vortices and skyrmions: Theory and computations, 2013. Available online at https://www.fgarciasanchez.es/thesisfelipe/node13.html#eq:etot.

[29] A. Vansteenkiste, J. Leliaert, M. Dvornik, M. Helsen, F. Garcia-Sanchez, and B. Van Waeyenberge. The design and verification of mumax3. *AIP Advances*, 4(10):107133, 2014.

[30] Tongyao Zhang, Yuansen Chen, Yanxu Li, Zhichao Guo, Zhi Wang, Zheng Han, Wei He, and Jing Zhang. Laser-induced magnetization dynamics in a van der waals ferromagnetic cr2ge2te6 nanoflake. *Applied Physics Letters*, 116(22):223103, 2020.

[31] Jeroen Mulkers. Vimag - an ovf data visualizer. https://github.com/jeroenmulkers/mumax-view, 2020.

9 Appendix

9.1 Extra images

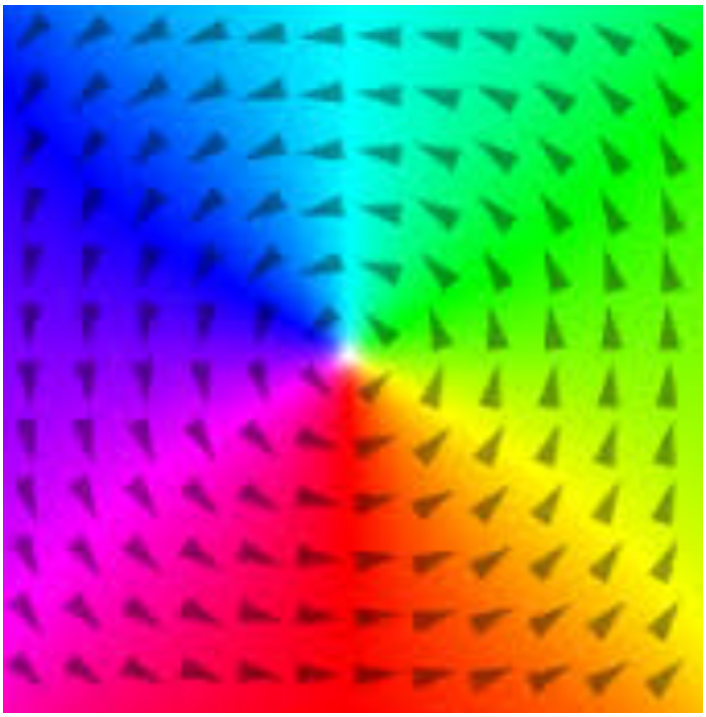

Figure 15: Visualization of each direction colour in Mumax3.

9.2 Mumax3 script

9.2.1 One domain

Magnetic cube sample is simulated through this script. // are comments, explaining what each line does.

```
setPBC(2, 2, 2) //Periodic boundary conditions
SetGridsize(50, 50, 50) //Grid size in cell number
SetCellsize(1e-9, 1e-9, 1e-9) //cell size in m
Msat = 500e3 // saturation magnetization
alpha = 0.02 // damping factor
m = uniform(0, 1, 0) // Initial magnetic moment directions
relax()
autosave(m, 10e-12)
tableautosave(10e-12)
B_ext = vector(400e-3, 0, 0) // External magnetic field direction and strength in T
OutputFormat = OVF2_TEXT
run(1e-9) //Running time in s
```

9.2.2 Two domains

Here the sample is split, where each half is set to a different K value.

```
SetPBC(1, 1, 0)
SetGridSize(40, 40, 10)
```

```
SetCellSize(1e-9, 1e-9, 1e-9)
Msat = 500e3
Aex = 1e-10
alpha = 0.02
defregion(1, xrange(0, 20e-9))
defregion(2, xrange(20e-9, 40e-9))
Ku1.setregion(1, 0.34e5)
anisU.setRegion(1, vector(1, 0, 0))
Ku1.setregion(2, 2*0.34e5)
anisU.setRegion(2, vector(1, 0, 0))
m.setRegion(1, uniform(0, 1, 0))
m.setRegion(2, uniform(0, 1, 0))
relax()
B_ext = vector(200e-3, 0, 0)
autosave(m, 10e-12)
tableautosave(10e-12)
OutputFormat = OVF2_TEXT
run(1e-9)
```

9.3 Python scripts

9.3.1 One domain

```
def parse_ovf_file(file_path):
    mx_list, my_list, mz_list = [], [], []

    with open(file_path, 'r') as file:
        for line in file:
            if line.startswith('#'):
                continue

            match = re.match(r'(\S+)\s+(\S+)\s+(\S+)', line)
            if match:
                mx, my, mz = map(float, match.groups())
                mx_list.append(mx)
                my_list.append(my)
                mz_list.append(mz)

    avg_mx = sum(mx_list) / len(mx_list)
    avg_my = sum(my_list) / len(my_list)
    avg_mz = sum(mz_list) / len(mz_list)

    return avg_mx, avg_my, avg_mz

def extract_and_calculate_averages(folder_path):
    avg_mx_list, avg_my_list, avg_mz_list = [], [], []
    time_values = []

    for file_index, filename in enumerate(os.listdir(folder_path)):
        file_path = os.path.join(folder_path, filename)
```

```
        if os.path.isfile(file_path) and filename.endswith('.ovf'):
            avg_mx, avg_my, avg_mz = parse_ovf_file(file_path)

            avg_mx_list.append(avg_mx)
            avg_my_list.append(avg_my)
            avg_mz_list.append(avg_mz)

            # Convert file index to time value (assuming 10e-12 s per file index)
            time_values.append(file_index * 10e-12)

    return time_values, avg_mx_list, avg_my_list, avg_mz_list


def calculate_frequency(time_values, avg_values):
    # Perform Fast Fourier Transform (FFT)
    fft_values = np.fft.fft(avg_values)
    fft_freq = np.fft.fftfreq(len(time_values), time_values[1] - time_values[0])
    max_index = np.argmax(np.abs(fft_values))
    frequency = np.abs(fft_freq[max_index])

    return frequency
```

9.3.2 Two domains

```
def parse_ovf_file_2(file_path):
    mx_list_half1, my_list_half1, mz_list_half1 = [], [], []
    mx_list_half2, my_list_half2, mz_list_half2 = [], [], []

    with open(file_path, 'r') as file:
        for line_index, line in enumerate(file):
            if line.startswith('#'):
                continue
            match = re.match(r'(\S+)\s+(\S+)\s+(\S+)', line)
            if match:
                mx, my, mz = map(float, match.groups())
                if line_index % 40 < 20:  # First, third, fifth, etc., 20 lines
                    mx_list_half1.append(mx)
                    my_list_half1.append(my)
                    mz_list_half1.append(mz)
                else:  # Second, fourth, sixth, etc., 20 lines
                    mx_list_half2.append(mx)
                    my_list_half2.append(my)
                    mz_list_half2.append(mz)

    avg_mx_half1 = sum(mx_list_half1) / len(mx_list_half1)
    avg_my_half1 = sum(my_list_half1) / len(my_list_half1)
    avg_mz_half1 = sum(mz_list_half1) / len(mz_list_half1)
    avg_mx_half2 = sum(mx_list_half2) / len(mx_list_half2)
    avg_my_half2 = sum(my_list_half2) / len(my_list_half2)
    avg_mz_half2 = sum(mz_list_half2) / len(mz_list_half2)
```

```
    return (avg_mx_half1, avg_my_half1, avg_mz_half1),

    (avg_mx_half2, avg_my_half2, avg_mz_half2)

def extract_and_calculate_averages_2(folder_path):
    avg_mx_list_half1, avg_my_list_half1, avg_mz_list_half1 = [], [], []


    avg_mx_list_half2, avg_my_list_half2, avg_mz_list_half2 = [], [], []
    time_values = []

    for file_index, filename in enumerate(sorted(os.listdir(folder_path),

    key=lambda x: os.path.getmtime(os.path.join(folder_path, x)))):
        file_path = os.path.join(folder_path, filename)

        if os.path.isfile(file_path) and filename.endswith('.ovf'):
            (avg_mx_half1, avg_my_half1, avg_mz_half1),

            (avg_mx_half2, avg_my_half2, avg_mz_half2) = parse_ovf_file_2(file_path)

            avg_mx_list_half1.append(avg_mx_half1)
            avg_my_list_half1.append(avg_my_half1)
            avg_mz_list_half1.append(avg_mz_half1)
            avg_mx_list_half2.append(avg_mx_half2)
            avg_my_list_half2.append(avg_my_half2)
            avg_mz_list_half2.append(avg_mz_half2)

            time_values.append(file_index * 10e-12)

    return time_values, (avg_mx_list_half1, avg_my_list_half1, avg_mz_list_half1),

    (avg_mx_list_half2, avg_my_list_half2, avg_mz_list_half2)
```